Freeze-Dried Precursor-Based Synthesis of Nanostructured Cobalt−Nickel Molybdates $Co_{1-x}Ni_xMoO_4$

David Vie, Eduardo Martínez, Fernando Sapiña,* José-Vicente Folgado, and Aurelio Beltrán

Institut de Ciència dels Materials de la Universitat de València, P.O. Box 2085, E-46071 València, Spain

Rita X. Valenzuela† and Vicente Cortés-Corberán

Instituto de Catálisis y Petroleoquímica, CSIC, Marie Curie s/n, Cantoblanco, E-28049 Madrid, Spain

Received October 28, 2003. Revised Manuscript Received February 24, 2004

A simple processing route to nanostructured mixed cobalt−nickel molybdates, $Co_{1-x}Ni_xMoO_4$ ($0 \leq x \leq 1$), has been developed. It is based on the use of precursors resulting from the freeze-drying of aqueous solutions of the appropriate common metal salts. Thermal decomposition of amorphous freeze-dried powders at low temperatures produces the nanostructured mixed oxides. A study of the influence of the preparative variables on the outcomes of this procedure is presented. The resulting materials have been characterized by X-ray powder diffraction, elemental analysis, scanning electron microscopy, thermogravimetry under oxygen flow, and physisorption measurements. $Co_{1-x}Ni_xMoO_4$ grains (obtained by calcination below 773 K) are aggregates of nanometric particles (with diameters typically around 30−40 nm) and have relatively high specific surface areas (20−40 m^2/g). The catalytic activity of the nanostructured cobalt and nickel molybdates for the oxidative dehydrogenation of propane has been evaluated. The performance of these nanostructured catalysts in this process is higher than those reported for homologous oxides prepared through conventional procedures.

Introduction

Nanostructured materials are ultrafine grained solids with a high proportion of atoms at grain boundaries. This kind of material plays an important role in nanotechnology, an emerging field covering different approaches devoted to exploit the novel physical and chemical properties that arise in solid systems whose sizes are intermediate between isolated atoms or molecules and bulk materials.[1]The possible applications for which these new materials are being investigated really are impressive. Among the research topics in progress are catalysts and catalytic supports able to drive more efficient and environmental-friendly processes, ceramic nanoparticles-reinforced composite materials, improved-performance anodes and cathodes for rechargeable lithium-ion batteries, or photoelectrochemical cells for energy supply based on nanostructured ceramics.[1,2]

In any case, the key factor for industrial exploitation of nanostructured materials lies on the development of cost-effective, large-scale manufacturing processes.[1,2] At present, more than 2 dozen different processes for their preparation have been described. However, most of these methods are expensive, require sophisticated equipment, and yield relatively low production rates. Therefore, they have high production costs and are conceived for obtaining high value-added materials, with typical applications in the fields of electronics and photonics. In other cases, difficulties may appear owing to operation details. Indeed, a problem frequently associated with sol−gel-related methods lies in the stoichiometric control and the cationic distribution in multicomponent systems.

In the past few years, we have developed preparative routes to different types of materials on the basis of the thermal decomposition of precursors obtained by freeze-drying of stable solutions.[3] A judicious election of the solvent and the source compounds allows one to obtain,

* To whom correspondence should be addressed. E-mail: fernando.sapina@uv.es.

† Present address: Centro de Investigaciones Energéticas, Medioambientales y Tecnológicas, CIEMAT, Avda. Complutense 22, 28040 Madrid, Spain.

(1) (a) The Interagency Working Group on Nanoscience, Engineering and Technology. *National Technology Initiative: Leading to the Next Industrial Revolution*; Committee on Technology, National Science and Technology Council: Washington, DC, 2000. (b) The Interagency Working Group on Nanoscience, Engineering and Technology. *Nanostructure Science and Technology: a Worldwide Study*; Committee on Technology, National Science and Technology Council, Loyola College in Maryland, Lexington, 1999. (c) *Nanotechnology: a Special Report*, *C&EN* **2001**, Oct 16, 25.

(2) (a) Tahyer, A. M. *C&EN* **2001**, Nov 26, 13. (b) Ouellette, J. *Ind. Phys.* **1997**, *2*, 15.

(3) (a) Ng-Lee, Y.; Sapiña, F.; Martinez-Tamayo, E.; Folgado, J. V.; Ibañez, R.; Lloret, F.; Segura, A. *J. Mater. Chem.* **1997**, *7*, 1905. (b) Boix, T.; El Fadli, Z.; Sapiña, F.; Martinez, E.; Beltrán, A.; Vergara, J.; Ortega, R. J.; Rao, K. V. *Chem. Mater.* **1998**, *10*, 1569. (c) El-Fadli, Z.; Coret, E.; Sapiña, F.; Martinez, E.; Beltrán, A.; Beltrán, D. *J. Mater. Chem.* **1999**, *8*, 1793. (d) El-Himri, A.; Sapiña, F.; Ibañez, R.; Beltrán, A. *J. Mater. Chem.* **2001**, *11*, 2311. (e) Vie, D.; Valero, N.; Martínez, E.; Sapiña, F.; Folgado, J. V.; Beltrán, A. *J. Mater. Chem.* **2002**, *12*, 1017.

10.1021/cm035079w CCC: $27.50
Published on Web 04/08/2004

in many cases, amorphous disordered precursors. These precursors usually show high reactivity and chemical homogeneity, while their stoichiometry can be easily controlled and adjusted to the required composition of the final material. Moreover, the freeze-drying procedure makes use of simple equipment already utilized in different productive sectors and yields high production rates at comparatively low production costs.[4] In practice, benefiting from the high reactivity of these precursors, we have been able to prepare a diversity of materials by short-time, low-temperature thermal treatments. Besides, starting from a given precursor, in some cases it becomes possible to lead the synthesis to chemically different materials (intermetallic compounds, oxides, nitrides/oxynitrides, or carbides) by controlling the reaction atmosphere. In addition, in most cases we obtain nanostructured materials, that is, grains composed by a large number of particles with typical dimensions below 100 nm.[5]

In the present work, we report on how the use of freeze-dried precursors has allowed us to prepare nanostructured mixed oxides in the solid solution series $Co_{1-x}Ni_xMoO_4$. These materials are attractive as far as they have proved to be active in the oxidative dehydrogenation (ODH) of ethane, propane, and butane.[6] We have evaluated the catalytic activity of both the nanostructured cobalt and nickel molybdates in the ODH of propane. The results show that these materials are more efficient than the homologous molybdates obtained by other synthetic procedures.

Experimental Section

Synthesis. Materials used as reagents in the current investigation were $Co(NO_3)_2 \cdot 6H_2O$ (Panreac, 98.0%), $Ni(NO_3)_2 \cdot 6H_2O$ (Fluka, 98%), and $(NH_4)_6Mo_7O_{24} \cdot 4H_2O$ (Panreac, 99.0%). The starting Co-, Ni-, or Mo-containing solutions were prepared by dissolving their respective salts in distilled water. Then, they were combined to obtain (Co, Ni)−Mo source solutions having a total cationic concentration of 0.25 M, a total volume of 112 mL, and nominal molar compositions $Co_{1-x}Ni_xMo$ (x = 0.000, 0.125, 0.250, 0.375, 0.500, 0.675, 0.750, 0.875, 1.000). The masses of the different reagents were adjusted to obtain 3 g of the final products. A small amount of nitric acid was added to the solution (until pH ca. 1.15) after mixture to ensure long-term stability of the solutions. Droplets of these solutions were flash frozen by projection onto liquid nitrogen and then freeze-dried at a pressure of 1−10 Pa and at a temperature of 228 K in a Telstar Cryodos freeze-dryer. In this way, dried solid precursors were obtained as amorphous (X-ray diffraction) loose powders. Thermal evolution of the precursors was monitored by means of thermogravimetric experiments under an oxygen atmosphere (heating rate 5 K min^{-1}, flow rate 50 cm^3 min^{-1}), carried out using a Perkin-Elmer 7 system.

$Co_{1-x}Ni_xMoO_4$ samples were synthesized by thermal decomposition of the amorphous precursor solids. A sample of the selected precursor (ca. 0.5 g) was placed into an alumina boat and introduced in the furnace. Several runs under different experimental conditions were performed to determine the appropriate conditions for the preparation of the samples. The precursor powder was heated at 5 K min^{-1} to a final temperature T_f (T_f = 573, 673, 773, 873, and 973 K) that was held for a period of time t_{hold} (t_{hold} = 1, 5, 12, 24 h) under flowing oxygen. Then, the solid was cooled, leaving the sample inside the furnace (slow cooling, ca. 2 K min^{-1}). All products were stored in a desiccator over $CaCl_2$.

For comparative purposes, stoichiometric nickel and cobalt molybdates were prepared by coprecipitation. In accordance with previous reports,[6b,c] the molybdates were precipitated from the acidified (Co, Ni)−Mo source solutions by addition of a NH_4OH aqueous solution at 333 K. The solvent was evaporated under reduced pressure at 353 K, and the remaining solid was dried at 393 K for 12 h and calcined in air at 823 K for 5 h.

Elemental Analysis. Metal ratios in the solids were determined by energy-dispersive analysis of X-ray (EDAX) on an Hitachi S-4100 scanning electron microscope using a Röntec EDR 288 detector with quantification performed using virtual standards on associated EDWIN software. The operating voltage was 30 kV, and the energy range of the analysis was 0−20 keV.

X-ray Diffraction. X-ray powder diffraction (XRD) patterns were obtained from a Siemens D501 automated diffractometer using graphite-monochromated Cu Kα radiation. Routine patterns for phase identification were collected with a scanning step of 0.08° in 2θ over the angular range 2θ 10−70° with a collection time of 5 s/step. The cell parameters, and thus the cell volume of each product (T_f = 673 K, t_{hold} = 5 h), were obtained by profile fitting of the pattern using the Le Bail's method,[7] as implemented in the FULLPROF program,[8] from patterns collected with a scanning step of 0.02° in 2θ over the same angular range (2θ 10−70°) and with a longer acquisition time (10 s/step) to enhance statistics. The fits were performed using a pseudo-Voigt peak-shape function. In the final runs, the usual profile parameters (scale factors, background coefficients, zero points, half-widths, pseudo-Voigt, and asymmetry parameters for the peak shape) were refined. All graphical representations relating to X-ray powder diffraction patterns were performed using the DRXWin Program.[9]

Microstructural Characterization. The morphology of the products was observed using a scanning electron microscope (Hitachi S-4100) operating at an accelerating voltage of 30 kV. All the preparations were covered with a thin film of gold for better image definition.

Surface Areas. Physisorption measurements were performed with a Micromeritics ASAP 2000 instrument. The BET surface areas of the products obtained at 673 K (t_{hold} = 5 h) were determined by nitrogen adsorption at 77 K assuming a cross-sectional area of 0.162 nm^2 for the nitrogen molecule. Prior to adsorption measurements, the samples were outgassed in a vacuum at 423 K for 18 h.

Catalytic Activity. Two samples of each nanostructured single molybdate were evaluated: the cobalt molybdates (x = 0) prepared at 573 and 673 K (t_{hold} = 5 h) and the Ni molybdates prepared at 673 and 773 K (t_{hold} = 5 h). All the samples were tested for the ODH of propane at atmospheric pressure in a conventional flow, fixed-bed quartz reactor, at 673−798 K. Mixtures of propane (2 mol %), oxygen (4.6 mol %), and helium (balance) were fed to the reactor with a residence time of 70 g h/mol of C_3H_8, using a catalyst load of 0.5 g (particle size 0.25−0.42 mm) mixed with SiC bits (dilution

(4) King, C. J. *Freeze-Drying of Foods*; Chemical Rubber Publishing: Cleveland, OH, 1971.

(5) (a) Ng Lee, Y.; Sapiña, F.; Martinez, E.; Folgado, J. V.; Cortés Corberán, V. *Stud. Surf. Sci. Catal.* **1997**, *110*, 747. (b) Ng Lee, Y.; El-Fadli, Z.; Sapiña, F.; Martinez-Tamayo, E.; Cortés Corberán, V. *Catal. Today* **1999**, *52*, 45. (c) El-Himri, A.; Cairols, M.; Alconchel, S.; Sapiña, F.; Ibañez, R.; Beltrán, D.; Beltrán, A. *J. Mater. Chem.* **1999**, *9*, 3167. (d) El Himri, A.; Sapiña, F.; Ibañez, R.; Beltrán, A. *J. Mater. Chem.* **2000**, *10*, 2537. (e) Valenzuela, R. X.; Bueno, G.; Solbes, A.; Sapiña, F.; Martínez, E.; Cortés-Corberán, V. *Top. Catal.* **2001**, *15*, 181.

(6) (a) Kaddouri, A.; Anouchinsky, R.; Mazzocchia, C.; Madeira, L. M.; Portela, M. F. *Catal. Today* **1998**, *40*, 201. (b) Mazzocchia, C.; Aboumrad, C.; Diagne, C.; Tempesti, E.; Herrmann, J. M.; Thomas, G. *Catal. Lett.* **1991**, *10*, 181. (c) Stern, D. L.; Grasselli, R. K. *J. Catal.* **1997**, *167*, 550. (d) Maldonado-Hódar, F. J.; Palma, L. M.; Farinha, M. *J. Catal.* **1996**, *164*, 399.

(7) Le Bail, A.; Duroy, H.; Fourquet, J. L. *Mater. Res. Bull.* **1988**, *23*, 447.

(8) Rodriguez-Carvajal, J. *FULLPROF: A Program for Rietveld Refinement and Pattern Matching Analysis*, Abstracts of the Satellite Meeting on Powder Diffraction of the XV Congress of the IUCr, Toulouse, France, 1990; p 127.

(9) Primo, V. *Powder Diffr.* **1999**, *14*, 70.

1:4 v/v) to reduce the heat release per unit volume. Both the reactants and products were analyzed by gas chromatography on a Varian 3400 equipment, using a thermal conductivity detector and Porapak QS (3 m) and molecular sieve 13X (1 m) columns. In all reaction conditions, the mass and carbon balances were within 100 ± 2%.

Results and Discussion

First-series transition-metal molybdates (Mn, Fe, Co, Ni, and Zn) can present three different monoclinic structures. At high pressures (higher than 60 kbar), they adopt the relatively dense $NiWO_4$-type (*wolframite*) structure, with both cation types occupying a portion of octahedral holes in a hexagonal *pseudo* closest-packing of oxygen atoms.[10] The other two more open structures, which are the relevant ones in this work, are usually referred to as α-$MnMoO_4$-type and α-$CoMoO_4$-type structures. Both of them can be described on the basis of a defective cubic closest-packing of oxygen atoms, with one vacant per each nine anionic positions. They differ in the coordination environment of molybdenum atoms. These show a distorted tetrahedral coordination in the α-$MnMoO_4$-type structure, while they are octahedrally coordinated in the relatively denser α-$CoMoO_4$-type structure. On the other hand, the partner cations (like Mn or Co) have approximately octahedral coordination in both structural types.[11]

Under atmospheric pressure, both the Co and Ni molybdates can adopt two different polymorphic forms, α and *β*. It is rather noteworthy that their relative thermal stabilities be exactly the opposite each other. Thus, in the Co case, the low-temperature form is the mauve *β*-$CoMoO_4$, which has the α-$MnMoO_4$-type structure. The dark green α-$CoMoO_4$ is the high-temperature form, and it defines the structural type that takes its name. This α-$CoMoO_4$ phase can be partially stabilized (i.e., as a mixture with *β*-$CoMoO_4$) at room temperature by quenching. On the other hand, a slight increase in pressure promotes a partial transition from *β*-$CoMoO_4$ to α-$CoMoO_4$.[12,6c] In contrast, in the Ni case, the low-temperature form is the green α-$NiMoO_4$ phase (α-$CoMoO_4$-type structure), which turns into the deep yellow *β*-$NiMoO_4$ (α-$MnMoO_4$-type structure) at relatively high temperatures. Stabilization of *β*-$NiMoO_4$ at room temperature only has been achieved up to date in the form of biphasic mixtures including NiO particles.[13]

Co−Mo System. The TG curve corresponding to the thermal evolution of the pure cobalt ($x = 0$) freeze-dried powder precursor displays two sharp partially superimposed mass losses. The first low-temperature step, which begins at 340−360 K, is associated with the evolution of nitric acid and/or water molecules retained in the precursor (and, probably, something of ammonium nitrate). The second mass loss, which occurs in the approximate 423−553 K range, really corresponds to the thermal decomposition of the precursor.

The XRD patterns of some representative samples of the products resulting from the thermal treatment ($t_{hold} = 5$ h, dynamic oxygen atmosphere) of the pure cobalt precursor ($x = 0$) at temperatures ranging from 573 to 973 K are shown in Figure 1. The most remarkable feature in these patterns is the observation of *β*-$CoMoO_4$ (JCPDS Card 21-0868) as a single phase at a synthesis temperature as low as 573 K. In fact, single-phased *β*-$CoMoO_4$ is systematically obtained by thermal treatments of the solid precursor at 573 K during times ranging from only 1 to 24 h, and no additional crystalline phase is detected in the course of the transformation from the amorphous precursor into molybdate. This same result occurs at calcination temperatures up to 873 K. The α-$CoMoO_4$ phase (JCPDS 25-1434) becomes detectable as a minority phase at 973 K. We have carried out also a set of experiments to investigate the possibility of stabilizing single-phased α-$CoMoO_4$ at room temperature. It has not been possible, regardless the previous thermal treatment used.

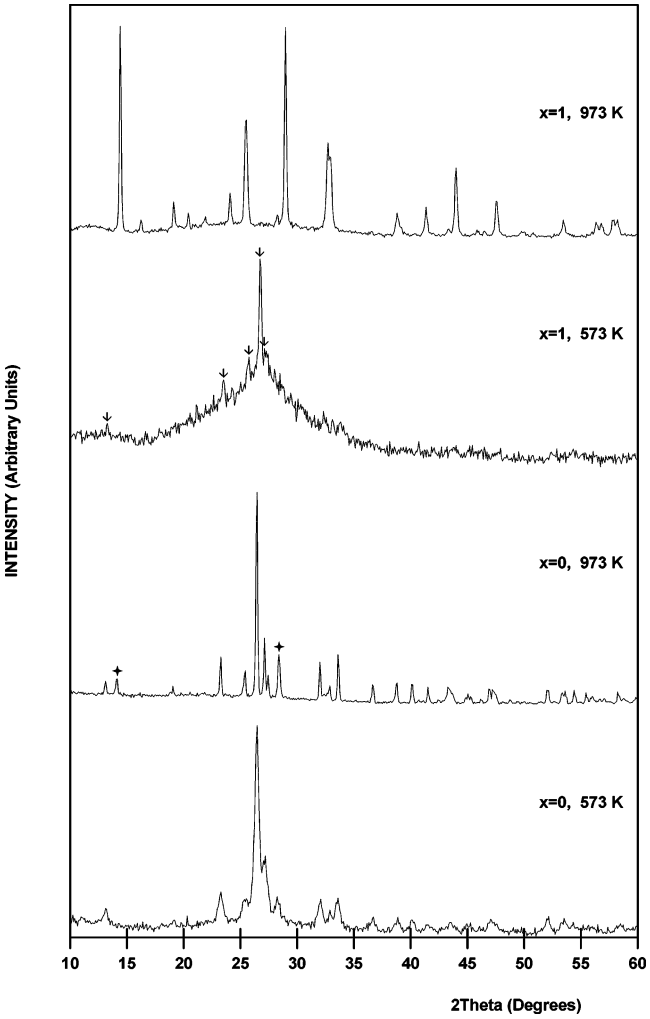

Figure 1. X-ray powder diffraction patterns of the products resulting from the thermal treatment (see text) of the $CoMoO_4$ ($x = 0$) and the $NiMoO_4$ ($x = 1$) freeze-dried precursors. For $x = 0$, all the patterns correspond to single-phased *β*-$CoMoO_4$, except that corresponding to the treatment at 973 K, in which the presence of an impurity of α-$CoMoO_4$ (+) is observed. For $x = 1$ the pattern at 573 K corresponds to *β*-$NiMoO_4$ (↓). The remaining patterns correspond to α-$NiMoO_4$.

Characteristic SEM images corresponding to *β*-$CoMoO_4$ samples prepared at 573 and 873 K ($t_{hold} = 5$ h) are shown in Figure 2. The samples prepared at 573 and 673 K consist of aggregates of spherical particles with typical diameters below 30 nm (a result consistent with calculations based on the fwhm values of the peaks

(10) Young, A. P.; Schwartz, C. M. *Science* **1963**, *141*, 348.
(11) Sleight, A. W. *Acta Crystallogr. B* **1972**, *28*, 2899.
(12) Sleight, A. W.; Chamberland, B. L. *Inorg. Chem.* **1968**, *7*, 1673.
(13) Mazzocchia, C.; Di Renzo, F.; Aboumrad, Ch.; Thomas, G. *Solid State Ionics* **1989**, *32*, 228.

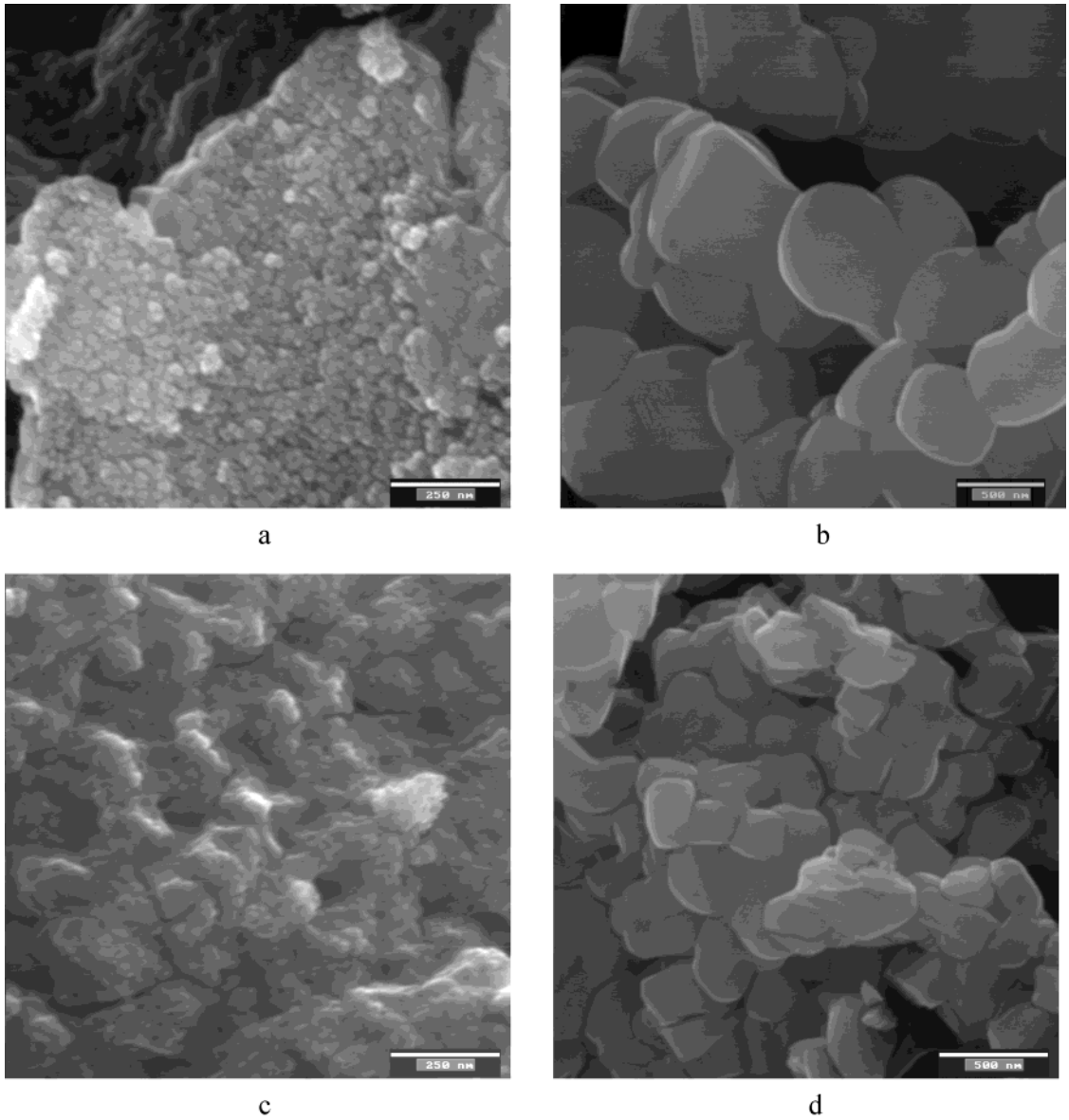

Figure 2. SEM images showing the microstructure of $CoMoO_4$ prepared at (a) 573 and (b) 873 K and of $NiMoO_4$ prepared at (c) 673 and (d) 973 K. Scale bars correspond to 250 nm (a and c) and 500 nm (b and d).

in the XRD patterns).[14] It seems that, in this temperature range, the growth of the particles is inhibited. At 773 K, the particles have experienced a certain growth, with typical diameters around 80 nm. Finally, at 873 K, some grain sintering is observed; the particles, which have significantly grown (typical mean size around 500 nm), are already polyhedral faceted.

On the other hand, we have carried out additional experiments on precursor samples corresponding to $CoMo_yO_4$ ($0.90 \leq y \leq 1.11$) nominal compositions to investigate possible effects associated with nonstoichiometry. In the solids prepared at 973 K, the only remarkable effect in this context is the relative increase of the α/β ratio (the α phase begins to appear as the majority one) with the cobalt deficit (i.e., $y > 1$).

Ni−Mo System. Like the Co−Mo system, the TG curve corresponding to the thermal evolution of the pure nickel ($x = 1$) freeze-dried powder precursor shows three mass losses. The first two steps (which occur at temperatures similar to the former case) are sharp and appear superimposed. As above, they could be associated with the evolution of physisorbed molecules and the thermal decomposition of the major portion of the precursor. Then, a relatively less pronounced mass loss occurs at 600−785 K. It might be related to the decomposition of some Ni-containing species, not completed at lower temperatures (a result which is consistent with the TG data corresponding to (Co, Ni)−Mo precursors, see below).

The XRD patterns of some representative samples of the products resulting from the thermal treatment ($t_{hold} = 5$ h, dynamic oxygen atmosphere) of the stoichiometric $x = 1$ precursor are shown in Figure 1. In light of the above structural comments, a rather noticeable result is the observation, at a synthesis temperature of 573 K, of single-phased β-$NiMoO_4$ (JCPDS 45-0142) as the first formed crystalline variety (although the material

(14) The size of the crystallites has been calculated from XRD patterns by a standard Scherrer analysis of the half-width of the XRD peaks, using well-crystallized $Pb(NO_3)_2$ as standard to calibrate the intrinsic width associated with the equipment. A detailed description of the procedure can be found in ref 15.

shows a poor crystallinity, i.e., broad diffraction peaks). However, at temperatures ranging from 773 to 973 K, it is the α-$NiMoO_4$ polymorph (JCPDS 33-0948) which is obtained as single phase (even for treatment times as short as 1 h). At 673 K, a mixture of the α (majority) and β phases was observed. Additional experiments carried out at 573 K using longer treatment times (up to 24 h) confirm that β-$NiMoO_4$ is obtained as a single phase at this temperature. On the other hand, a mere increase of 50 K in the preparation temperature (T_f = 623 K) leads to mixtures of α and β phases after 5 h of thermal treatment. Finally, at 673 K, the relative amount of the β-$NiMoO_4$ phase decreases with the increase of the thermal treatment duration. In fact, α-$NiMoO_4$ is obtained as a nearly single phase after 24 h.

Figure 2 shows some characteristic SEM images corresponding to $NiMoO_4$ samples obtained at 673 and 973 K (t_{hold} = 5 h). The samples prepared at 673 and 773 K present very porous surfaces, which are built from aggregates of spherical particles with a mean diameter around 40 nm. It seems that the growth of the particles formed at these temperatures is so limited that the precursor morphology is kept. The porous structure already has collapsed at 873 K, although the particles are still spherical, with a typical diameter close to 60 nm. Finally, at 973 K, we can observe polyhedral faceted particles with a mean particle size of 500 nm.

Experiments on samples corresponding to nonstoichiometric $NiMo_yO_4$ ($0.90 \leq y \leq 1.11$) compositions yield similar results concerning phase evolution with treatment temperature. However, MoO_3 peaks (JCPDS 05-0508) are observed in the patterns corresponding to Ni-deficient samples ($y > 1$) treated at temperatures ranging from 673 to 773 K (there is a certain phase segregation). In contrast, in the case of Ni-rich samples ($y < 1$), we do not observe (XRD patterns) additional phase segregation or further β-$NiMoO_4$ phase stabilization (which according to previous results should be favored, as mentioned above, in the presence of an excess of NiO). On the other hand, concerning grain morphology, nonstoichiometry results in a faster (i.e., at minor temperature) collapse of the porous structure, but the nanometric character of the particles is maintained for $T_f \leq 773$ K.

(Co, Ni)−Mo System. The TG curves corresponding to the evolution of the (Co, Ni)−Mo precursors look like that registered for the Ni−Mo system. They show three mass losses, and both the overlapping between the two first steps and the temperature at which the final process occurs (x = 0.125, 535−660 K; x = 0.875, 585−755 K) increase as the Ni content.

Figure 3 shows the XRD patterns of some representative samples of the products resulting from thermal treatments at temperatures ranging from 573 to 973 K (t_{hold} = 5 h, dynamic oxygen atmosphere) of the x = 0.375 and x = 0.875 precursors. In practice, their behaviors are representative of those observed for the entire compositional range ($0.125 \leq x \leq 0.875$).

In all cases, the solid obtained at 573 K is monophasic and has the β-type structure. On the other hand, the sample crystallinity increases (i.e., the width of the diffraction peaks decreases) with the Co content. At temperatures higher than 573 K, the nature of the

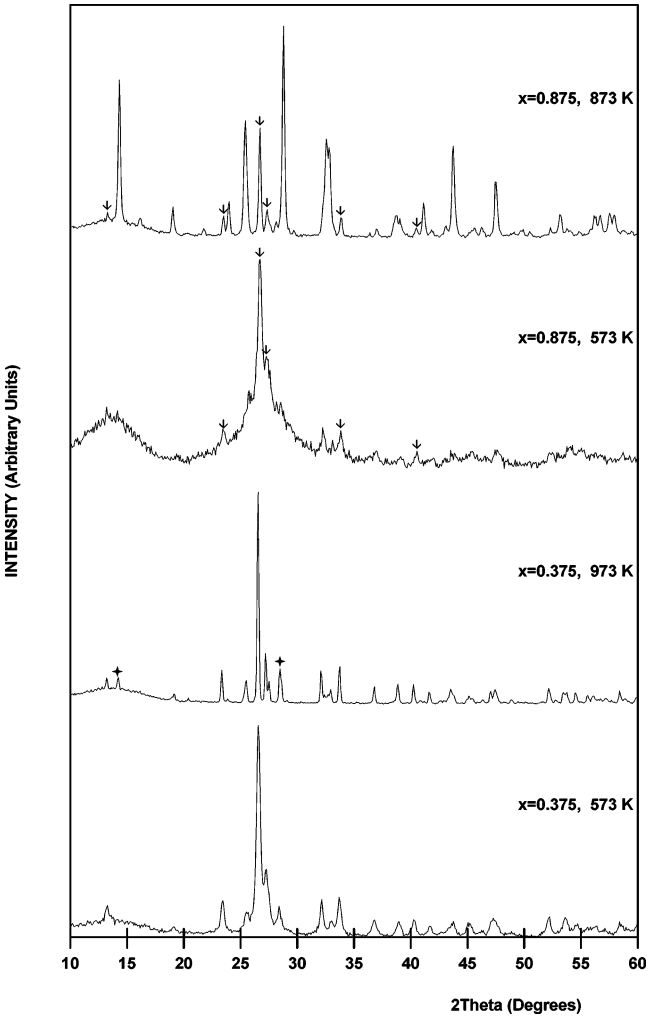

Figure 3. X-ray diffraction powder patterns of the products resulting from the thermal treatment (see text) of the x = 0.375 and the x = 0.875 freeze-dried precursors. For x = 0.375 all the patterns correspond to the β phase, except that corresponding to the treatment at 973 K, in which the presence of an impurity of the α phase (+) is observed. For x = 0.875, the patterns correspond to mixtures of the β (↓) and the α phases. The α phase is practically absent at 573 K, whereas it is the majority phase at 973 K.

products resulting from the thermal evolution of the precursors varies with their composition. Thus, in the case of the Co-rich samples ($x < 0.5$), the β phase results stabilized (the product is monophasic) up to 873 K. In fact, T_f must reach 973 K to observe some small diffraction peaks associated with the α phase, similarly to that observed for the Co−Mo system. The prevalence range of the β phase gets shorter as the Ni content increases. Thus, for $x \geq 0.5$, the presence of the α phase already is detected at 673 K, although the β phase remains as the major one below 773 K for all the compositions. The relative intensity of the diffraction peaks of the α phase increases with both T_f and the Ni content. In the Ni-rich end (x = 0.875), the α phase is clearly the majority one at 973 K, but in no case (under our experimental conditions) is it obtained as a single phase (in the presence of Co).

Concerning the products microstructure, the results are, in general, similar to those observed for the Co−Mo system. Below 773 K, the products are nanostructured and consist of aggregates of spherical particles

Table 1. Chemical Composition and BET Surface Area of $Co_{1-x}Ni_xMoO_4$ Samples Calcined at 673 K[a]

x (nominal)	*x* (EDAX)[b]	(Co + Ni):Mo (EDAX)[c]	BET surface area (m^2/g)
0.000		1.07	18
0.125	0.12	0.97	23
0.250	0.23	1.09	22
0.375	0.36	0.99	28
0.500	0.49	1.06	32
0.625	0.64	1.01	36
0.750	0.75	0.96	41
0.875	0.86	1.09	39
1.000		1.08	39

[a] Values averaged from data of 30 particles; spot area 0.5 μm. [b] Estimated absolute error in *x* is 0.04. [c] Estimated absolute error in (Ni + Co):Mo is 0.08.

with typical diameters around 40 nm. The particles have grown slightly at 773 K (typical diameters around 80 nm) and appear as polyhedral faceted at 873 K (with mean sizes around 500 nm).

Table 1 summarizes the results of the physisorption measurements performed on samples of the products obtained at 673 K (t_{hold} = 5 h, dynamic oxygen atmosphere). As can be noted, the resulting materials have, in all cases, relatively high surface areas (20−40 m^2/g). The geometrical surface area, *S*, calculated assuming that the particles are spherical and using typical diameters obtained by SEM (40 nm), is around 30 m^2/g ($S = 6000/\rho d$, where *S* is the geometrical surface area, in m^2/g, ρ the density, in g/cm^3, and *d* the typical diameter of the particles, in nm), which is in good agreement with the measured BET surface areas. Table 1 also includes the results of the corresponding EDAX elemental analyses. In all cases, both the Co/(Co + Ni) and the (Co + Ni)/Mo ratios fit in well (within experimental error) with the nominal ones in the respective precursors. On the other hand, within the limitations of the technique (diameter of the electron spot of 0.5 μm), no inhomogeneities in the distribution of Co and Ni in the samples were detected. Although inhomogeneities at smaller scale cannot be discarded a priori, we have calculated the cell volumes of the α and β phases for each sample (from the cell parameters obtained by profile fitting of the patterns using the Le Bail method) to confirm the existence of solid solutions. According to Vegard's Law, the cell volume should change linearly with the composition.[15] Figure 4 shows the dependence of the cell volume with the composition for the α and β phases in $Co_{1-x}Ni_xMoO_4$ samples. The linear variation in both cases confirms the homogeneous distribution of the Co and Ni cations in the samples.

Catalytic Properties. In the experimental conditions used, all the tested molybdate catalysts were active and selective for the oxidative dehydrogenation (ODH) of propane, producing conversions from 1 to 5% at 673 K up to 40% at 798 K with selectivities to propene between 90 and 40%. The only detected products were propene, CO_2, water, and traces of ethane and ethene. The apparent activation energy was practically the same for all the samples, around 20 ± 2 kcal/mol. For each molybdate system, the samples with higher catalytic activity (or conversion at a given temperature) were

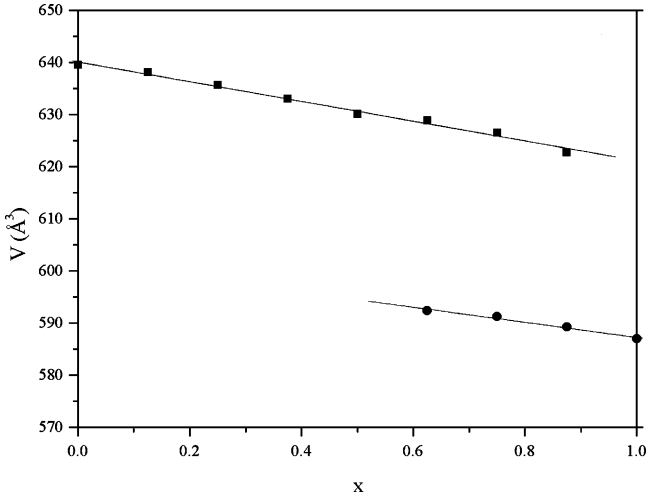

Figure 4. Cell volume versus composition for α and β phases in $Co_{1-x}Ni_xMoO_4$ samples. Solid lines correspond to the best linear fits to the data.

those prepared by calcination at the lower temperatures (573 K/5 h for Co−Mo and 673 K/5 h for Ni−Mo). This can be correlated with the higher values of the BET surface areas of these samples as compared to those prepared at higher temperatures.

Both surface areas and catalytic properties for ODH of propane of the molybdates prepared by freeze-drying are dependent on the transition metal cation. The specific surface area BET is little sensitive to the final calcination temperature (T_c) for the nickel molybdate, while it decreases with the increase of T_c for the cobalt molybdate. Selectivity values are higher for Co−Mo samples, in accordance with literature reports from other groups,[6] and the selectivity drop with the increase of conversion is faster for Ni−Mo samples.

For comparative purposes, we have measured the catalytic activity, under the same experimental conditions, of stoichiometric cobalt and nickel molybdates prepared by the conventional coprecipitation method (hereinafter denoted as CP).[6b,c,16] These samples had BET areas of 10 and 46 m^2/g, respectively. Whereas the surface areas are similar for both sample types in the Ni−Mo system, surface areas in the Co−Mo system are 2 times greater in samples prepared from freeze-dried precursors. For this reason, to study the influence of the preparation method on the catalytic properties, it is more meaningful to compare their catalytic activities in terms of area-specific rate, or intrinsic activities, to avoid the influence of the different surface areas.

As can be seen in Figure 5, the comparison of the intrinsic activity for ODH of propane of the nanostructured molybdate catalysts with their CP counterparts also depends on the nature of the transition metal (Ni or Co). Freeze-dried samples were more active among the nickel molybdate samples; at a variance, the cobalt molybdates showed a lower area-specific activity than their CP counterparts. Nevertheless, and even more relevant from the catalytic point of view, in both molybdate systems (and regardless of the calcination temperature) the freeze-dried samples show a much

(15) West, A. K. *Solid State Chemistry and its Applications*; John Wiley and Sons: Chichester, U.K., 1984.

(16) (a) Qin, D.; Valenzuela, R. X.; Muñoz Asperilla, J. M.; Wang, G. J.; Wu, T. H.; Cortés Corberán, V. In *Proceedings XV Iberoamerican Symposium on Catalysis*, Córdoba, Argentina, 1996; Vol. 3, p 1491. (b) Yoon, Y. S.; Fujikawa, N.; Moro-Oka, Y. *Chem. Lett.* **1994**, 1635.

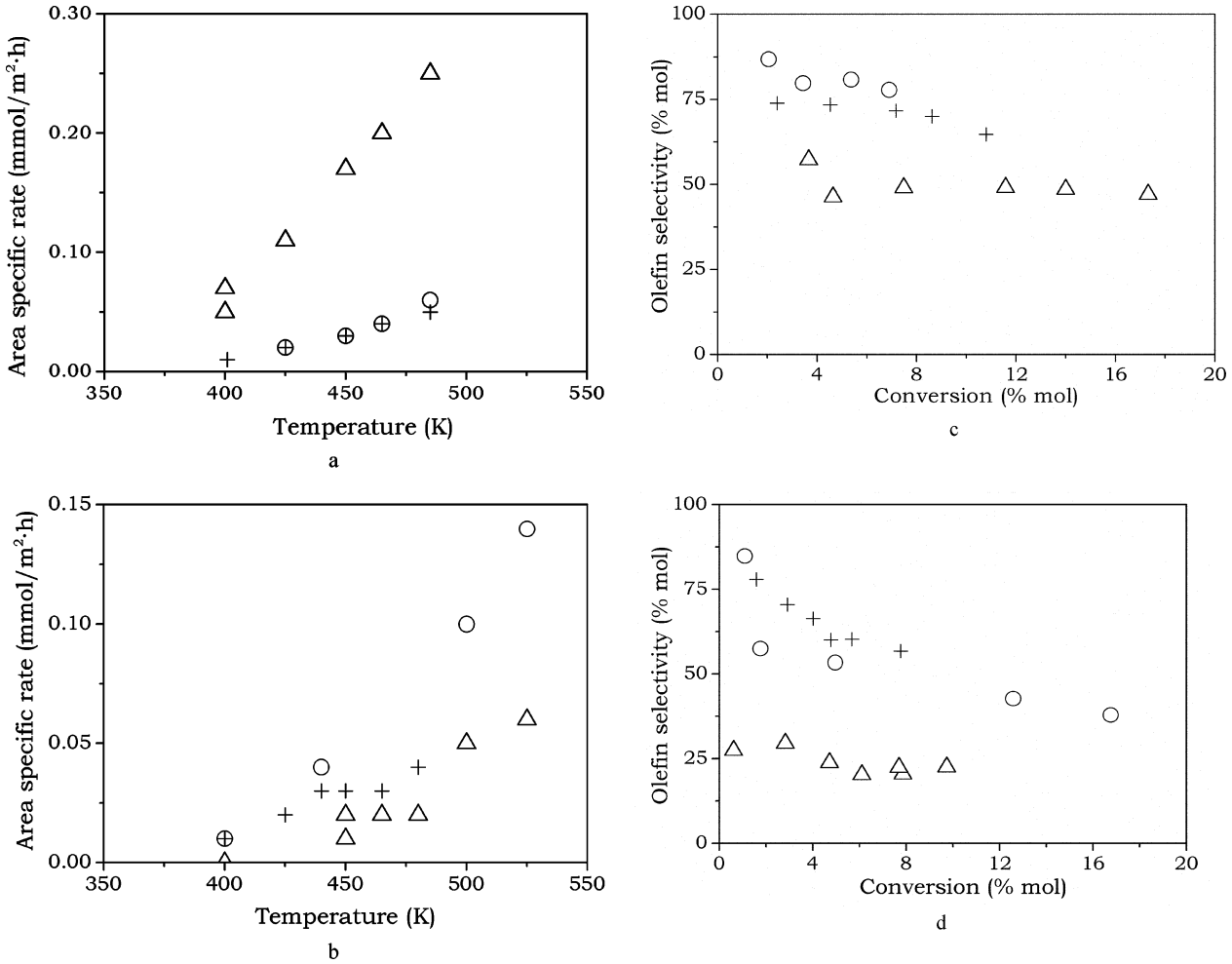

Figure 5. Catalytic performance of the $Co_{1-x}Ni_xMoO_4$ ($x = 0$, 1) prepared by the freeze-dried precursors method and their homologous molybdates prepared by coprecipitation (CP; open triangles). (a) Effect of the reaction temperature on the area specific rate for the $x = 0$ samples (+ and ○, samples prepared at 573 and 673 K, respectively). (b) Effect of the reaction temperature on the area specific rate for the $x = 1$ samples (+ and ○, samples prepared at 673 and 773 K, respectively). (c) Variation of selectivity to olefin as a function of propane conversion for the $x = 0$ samples (+ and ○, samples prepared at 573 and 673 K, respectively). (d) Variation of selectivity to olefin as a function of propane conversion for the $x = 1$ samples (+ and ○, samples prepared at 673 and 773 K, respectively).

better selectivity to the olefin, with an increase up to 20−25%. This represents a 30−50% increase of selectivity (at iso-conversion) for the cobalt-containing sample, and an increase by a factor of 2 to 3 for the $NiMoO_4$ samples. As a consequence, an increase of around 30−40% of yield of propene is obtained with the catalysts prepared by the freeze-drying method in comparison with their conventional counterparts. This substantial performance improvement deserves careful attention to use the freeze-drying synthesis method as a tool to optimize the preparation of selective molybdate catalysts.

Concluding Remarks

Thermal decomposition of amorphous freeze-dried powders at relatively low temperatures allows one to prepare nanostructured cobalt−nickel molybdates in the solid solution series $Co_{1-x}Ni_xMoO_4$ ($0 \leq x \leq 1$). The surface areas and the catalytic properties for ODH of propane of cobalt and nickel molybdates prepared in this way are dependent on the transition metal cation, being less sensitive to the final calcination temperature (T_c) for the nickel molybdate than for the cobalt molybdate. Compared to their homologous counterparts, prepared by the conventional coprecipitation method, these nickel molybdates are more active while the area specific rate of the cobalt molybdates is lower. However, in all cases the samples prepared via freeze-drying show a much higher selectivity to olefin at isoconversion, resulting in a great increase of around 30−40% of propene yield. In practice, this is an interesting result concerning the possibility of improving the performance of molybdate catalysts for ODH of light alkanes and, consequently, further studies on this subject are in progress.

Acknowledgment. This research was supported by the Spanish Ministerio de Ciencia y Tecnología (MAT99-0648, MAT2002-03803, and MAT 2003-01696). The SCSIE of the Universitat de València is acknowledged for X-ray diffraction and analytical facilities.

CM035079W